Artificial DNA: PNA & XNA 4:2, 58–68; April/May/June 2013; © 2013 Landes Bioscience

Rapid genotyping using pyrene–perylene locked nucleic acid complexes

T. Santhosh Kumar,[1,2] Anna Myznikova,[3] Evgeniya Samokhina[4] and Irina Kira Astakhova[1,*]

[1]Nucleic Acid Center; Department of Physics, Chemistry and Pharmacy; University of Southern Denmark; Odense, Denmark; [2]National Institute of Diabetes and Digestive and Kidney Diseases; National Institutes of Health; Molecular Recognition Section; Bethesda, MD USA; [3]Central Research Institute of Epidemiology; Moscow, Russia; [4]Russian Federal AIDS Centre; Moscow, Russia

Keywords: oligonucleotide, LNA, pyrene, perylene, fluorescence, FRET, SNP

Abbreviations: LNA, locked nucleic acid; PAH, polyaromatic hydrocarbon; SNP, single-nucleotide polymorphism; PIs, protease inhibitors; FRET, Förster resonance energy transfer

We have developed an assay for single strand DNA and RNA detection which is based on novel pyrene–perylene FRET pairs attached to short LNA/DNA probes. The assay is based on ratiometric emission upon binding of target DNA/RNA by three combinations of fluorescent LNA/DNA reporter strands. Specific geometry of the pyrene fluorophore attached to the 2'-amino group of 2'-amino-LNA in position 4 allows for the first time to efficiently utilize dipole–dipole orientation parameter for sensing of single-nucleotide polymorphisms (SNPs) in nucleic acid targets by FRET. Using novel probes, SNP detection is achieved with advantages of large Stokes shift (115 nm), high fluorescence quantum yields and low limit of target detection values (< 5 nM). Rapid and accurate genotyping of highly polymorphic HIV Pol cDNA and RNA fragments performed herein proves the possibility for broad application of the novel pyrene–perylene FRET pairs, e.g., in imaging and clinical diagnostics.

Introduction

As detailed single-nucleotide polymorphism (SNP) maps become more accessible, there is a growing understanding that rapid and efficient detection methods are required to bring SNP analysis into mainstream use in molecular diagnostics laboratories. Through constant developing of SNPs under the selectional pressure of the global use of antiviral therapy, RNA viruses such as HIV-1 have evolved complex mechanisms for resistance to treatment with drugs.[1,2] In modern complex anti-viral HIV-1/AIDS therapy, SNPs causing drug resistance to protease inhibitors (PIs) are some of the most important, that demand a change in treatment when the resistance is developed.[3,4] However, current SNP genotyping is a time-consuming and rather expensive procedure typically performed using sequencing or microarray techniques.[5]

Förster resonance energy transfer (FRET) is one of the major fluorescence effects applied in nucleic acid biosensing which has been studied thoroughly.[6-19] Being a physical process whereby the excited state energy of a donor molecule can be transferred to a neighboring acceptor fluorophore in the ground state, FRET can take place whenever the two fluorophores with sufficient spectral overlap between the donor fluorescence and acceptor absorbance are in close proximity (distance typically below 7 nm), and importantly, provided favorable donor–acceptor dipole–dipole orientation. FRET can be monitored quantitatively and in real time (e.g., real-time PCR),[20-26] with additional possibilities for multiplexing and growing applications in imaging in vivo.[10,13] Several FRET pairs have already been applied in SNP genomics in different assays, which have their own advantages and drawbacks (e.g., Taqman probes, molecular beacons, dye-labeled oligonucleotide ligation and template-directed dye-terminator incorporation).[27] However using mainly dye–quencher design of FRET probes, none of these assays explore an important dipole–dipole orientation factor, which is known to influence FRET significantly and therefore might be a useful tool in creating nucleic acid probes for clinical diagnostics and bioimaging.[28]

Recently, sensitive polyaromatic hydrocarbon (PAH) dyes attached to locked nucleic acids (2'-amino- and isomeric 2'-α-L-amino-LNA) have been proven to be effective for SNP analysis of highly polymorphic model and natural targets.[29-31] This was done using short LNA/DNA probes and terminal excimer interactions between two pyrene or (phenylethynyl)pyrene residues. High sensitivity of the PAH-LNA monomers to minor changes in local microenvironments such as SNPs is mainly caused by precise positioning of PAHs within the double-stranded nucleic acid complexes provided by attachment to a rigid bicyclic LNA skeleton. High binding affinity and selectivity to DNA/RNA targets and sensitivity to SNPs was however often accompanied by low quantum yield of the pyrene derivatives substituted at position 1 (monomer **M**[1], **Fig. 1**).[30]

Herein, we aimed at improving fluorescence properties of the pyrene attached to 2'-amino-LNA by alternating the position of

*Correspondence to: Irina Kira Astakhova; Email: ias@sdu.dk
Submitted: 03/29/13; Revised: 07/07/13; Accepted: 07/25/13
http://dx.doi.org/10.4161/adna.25903

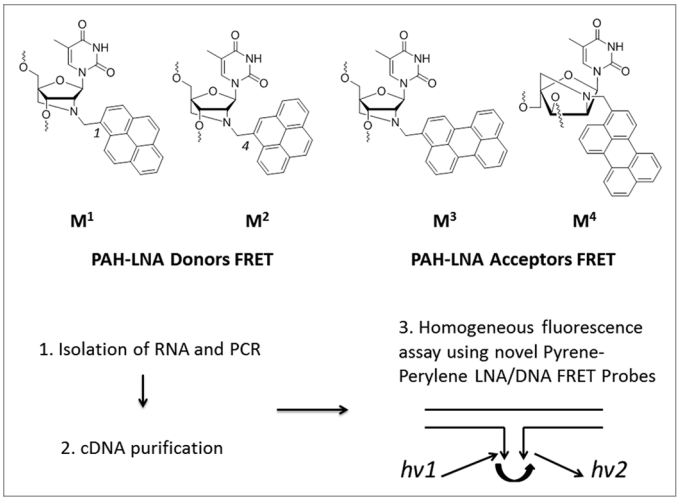

Figure 1. Chemical structures of modified PAH-LNA monomers **M**[1]–**M**[4] used in this study and homogeneous fluorescence assay for SNP detection using **M**[1]–**M**[4] within terminally labeled FRET probes.

substitution in the pyrene core from 1 to 4, since this modification has already showed promising results in labeling of nucleic acids (monomer **M**[2], **Fig. 1**).[31-34] We demonstrate that this modification significantly improved photophysical and spectral characteristics of the pyrene with a strong effect on its interactions with the commonly used PAH acceptor FRET perylene (monomers **M**[3] and **M**[4], **Fig. 1**).[35,36] We rationalized these results by molecular modeling studies and furthermore utilized the novel FRET pairs **M**[2]/**M**[3]–**M**[4] within short LNA/DNA probes for SNP sensing in cDNA fragments obtained from patients currently receiving anti-HIV-1/AIDS therapy (**Fig. 1**).

Results

Synthesis of monomer **M**[2] was performed starting from 2'-amino-LNA nucleoside **1**[37,38] and commercially available pyrene-4-carbaldehyde under reductive amination conditions[39] followed by phosphitylation[40] of **2** providing phosphoramidite **3** in 79% overall yield (**Scheme 1**). Previously investigated (pyrene-1-yl)methyl 2'-amino-LNA (monomer **M**[1]) was incorporated into oligonucleotides as a reference for the new FRET donor **M**[2,41] monomers **M**[3] and **M**[4] were prepared as previously described.[42,43]

For initial evaluation of pyrene–perylene FRET and SNP diagnostic potential, monomers **M**[1]–**M**[4] were incorporated in a model dual-probe FRET system **ON1**–**ON4** and covalently linked double-labeled analogs **ON5**–**ON8** adopted from previous research on PAH-LNA monomers (**Table 1**).[29,30] The model FRET probes were prepared using automated phosphoramidite DNA synthesis and first characterized by their melting temperatures with complementary and mismatched DNA/RNA targets (T_m; **Tables S1–S6**). Generally high melting temperatures of the short LNA/DNA probes **ON1**–**ON4** (37–63°C) were significantly decreased by mismatches in DNA and RNA targets located at the four neighboring positions to the modified monomers, while a single mismatch opposite to monomers **M**[1]–**M**[4] led

Table 1. Sequences and MALDI-MS of fluorescent oligonucleotides prepared in this study[a]

#	Sequence, 5'→3'	Found m/z [M-H]$^-$	Calc. m/z [M-H]$^-$
ON1	**M**[1]CT^L TCC AC^{L}A	3081	3082
ON2	**M**[2]CT^L TCC AC^{L}A	3083	3082
ON3	CA^{L}C CAA C**M**[3]	2685	2685
ON4	CA^{L}C CAA C**M**[4]	2685	2685
ON5	CA^{L}C CAA C**M**[3]**M**[1] CT^{L}T CCA C^{L}A	5732	5734
ON6	CA^{L}C CAA C**M**[3]**M**[2] CT^{L}T CCA C^{L}A	5730	5734
ON7	CA^{L}C CAA C**M**[4]**M**[1] CT^{L}T CCA C^{L}A	5731	5734
ON8	CA^{L}C CAA C**M**[4]**M**[2] CT^{L}T CCA C^{L}A	5734	5734
ON9	**M**[2]AT^L C^{L}T^{L}G^L C^{L}T^{L}C	3102	3102
ON10	**M**[2]G^{L}T^L A^{L}T^{L}C^L A^{L}T^{L}C	3139	3140
ON11	AT^{L}A^L C^{L}T^{L}G^L TA**M**[3]	3188	3186
ON12	AT^{L}A^L C^{L}T^{L}G^L TA**M**[4]	3186	3186
ON13	TT^{L}C^L T^{L}A^{L}A^L TA**M**[3]	3160	3161
ON14	TT^{L}C^L T^{L}A^{L}A^L TA**M**[4]	3158	3161

[a]T^L, thymin-1-yl LNA monomer; C^L, 5-methylcytosin-1-yl LNA monomer; G^L, guanin-9-yl LNA monomer; A^L, adenin-9-yl LNA monomer.

to small T_m changes in the complexes containing monomer **M**[2] displaying ΔT_m values of –0.5°C to +3.0°C (for example, T_m values of **ON2** upon binding DNA containing mismatch T→C at neighboring position 6 and mismatch A→C opposite to monomer **M**[2] were 19.0°C and 40.0°C, respectively; **Table S4**). Having compared T_m data for **ON1**–**ON2** and corresponding LNA/DNA reference 5'-(CA^L CCA ACT^L), we observed that the incorporated fluorophores had a large impact on mismatch discrimination in the two neighboring positions 6–7, although the duplexes were less destabilized and even stabilized for all the probes when a mismatch was opposite to the 3'-end nucleotide (**Tables S3–S4**). For example, T_m decrease upon binding RNA containing mismatch G→C at neighboring position 7 by **ON1**, **ON2** and reference LNA/DNA compared with fully complementary complexes (ΔT_m values) were –17.5°C, –19.5°C and ±0.0°C, respectively. However, ΔT_m values were –0.5°C, –0.5°C and +4.0°C for **ON1**, **ON2** and reference LNA/DNA, respectively, upon binding RNA target having A→U mismatch at position 8 (**Tables S3–S4**). As expected, all the longer hybrids **ON5**–**ON8** exhibited melting temperatures that were higher than 70°C and were generally less affected by mismatches compared with the dual probes **ON1**–**ON4** (**Fig. 2B**; e.g., T_m 71.0°C, 61°C and 70°C for duplexes of **ON7** with cDNA, DNA containing mismatch T→C at position 6 and mismatch A→C opposite to monomer **M**[1]; **Table S6**). The major differences between the T_m discrimination of the mismatched nucleotides in central and peripheral positions to monomers **M**[1]–**M**[4] can be attributed to several factors. First, owing to lower thermodynamic stability short fluorescent oligonucleotides generally display higher sensitivity of hybridization toward mismatched DNA/RNA targets than their longer analogs.[29-33] Second, flexibility of the terminally attached PAHs

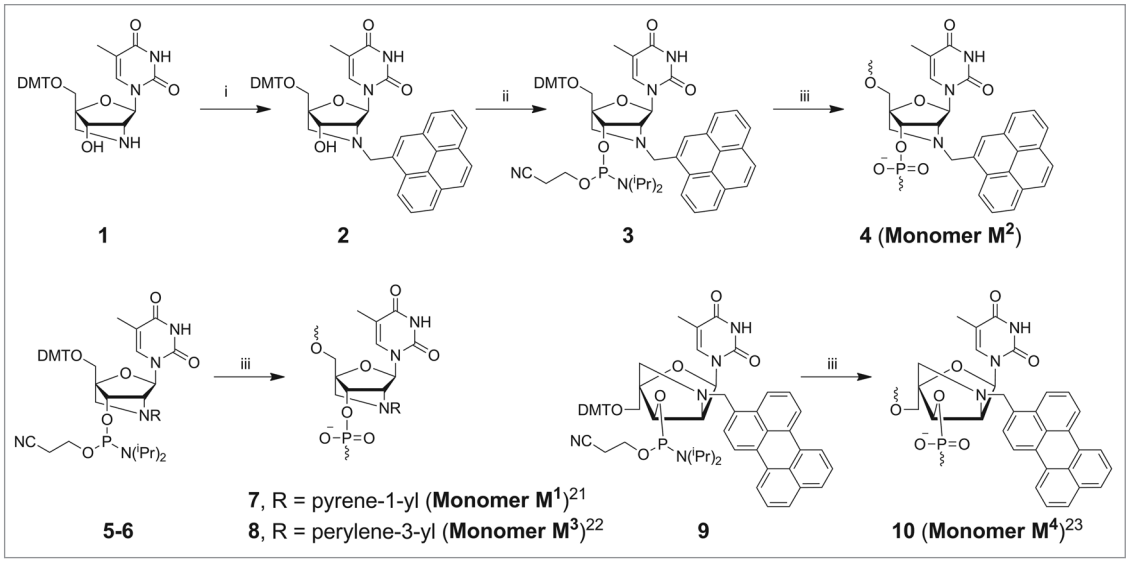

Scheme 1. Preparation of modified monomers M^1–M^4. Reagents, conditions (and yields): (i) pyrene-4-carbaldehyde, $NaBH(OAc)_3$, 1,2-dichloroethane, rt (87%); (ii) $NC(CH_2)_2OP(Cl)N(^iPr)_2$, DIPEA, CH_2Cl_2, rt (91%); (iii) DNA synthesizer. DMT, 4,4′-dimethoxytrityl.

might lead to better positioning of the bulky fluorophores within the dual-probe complementary duplexes with respect to those containing single-base mismatches leading to strongly decreased T_m values for the latter complexes. Third, increased stability of the duplexes containing mismatches opposite to modifications within the dual-probe format might result from proximity of the fluorophores to the end of the duplex, where fraying of the doubles-stranded complex diminishes the impact of mismatches relative to those located at internal positions.

Excitation was performed at 340 nm for all the FRET probes, since the monomers M^1 and M^2 revealed similar position and structure of their visible absorbance, excitation and fluorescence bands (**Table 2**). Photophysical and spectral properties of the model systems indicated superior quantum yields Φ_f 0.15–0.18 of M^2 compared with Φ_f 0.06–0.07 of M^1, although both FRET donors were quenched within single strands (**ON1**–**ON2**: Φ_f 0.04–0.05; **Fig. 2C and Table 2**). Fluorescence light-up upon hybridization points at the positioning of PAH fluorophores in nonpolar minor groove of the duplexes. Minor interactions of the fluorophores with the nucleobases within the complementary complexes were also confirmed by low sensitivity of the fluorophore's absorbance to the elevated temperature (**Fig. S3**). Moreover bright fluorescence of the complexes containing monomers M^2/M^3–M^4 contradicts intercalation typically leading to quenched PAH fluorescence due to interaction with nucleobases.[32]

The quantum yields and, hence, fluorescence brightness values FB of double-labeled probes **ON5**–**ON8** were very high (Φ_f 0.72–1.00 and FB up to 52.0), however without sensitivity of the fluorescence to single-base mismatches (**Fig. S1**). The mismatches were in turn strongly discriminated by dual-probes **ON2**–**ON4** containing M^2/M^3–M^4 FRET pairs (discrimination factor DF up to 16.7 using the ratio between fluorescence intensity of acceptor to donor; **Fig. S1**). Importantly, quantum yields of the donor FRET in absence of acceptor and extinction coefficient of the corresponding acceptor in absence of donor evaluated prior to FRET measurements were similar for fully complementary and singly-mismatched complexes (**Fig. S3**). High FRET efficiency values of the fully complementary complexes (E up to 1.00) were furthermore decreased in presence of a single mismatch opposite to the donor FRET M^2, but not opposite to acceptors M^3–M^4 (E 0.22–0.45 and 0.89–0.95, respectively; **Table S7**). Finally, mismatch discrimination in RNA targets was as efficient as in DNA, although with slight alterations of E and discrimination factor values, which can be attributed to the structural differences between the complexes with DNA and RNA.

Additional information about FRET can be obtained from calculation of donor–acceptor spectral overlap integral J and Förster distance R_0 (the donor–acceptor distance at which E = 50%), and from analysis of distance dependence of E values (**Fig. 3**).[28,44,45] The calculations were performed assuming dipole–dipole orientation factor χ^2 = 2/3 due to emission dipole of the donor and the absorption dipole of the acceptor randomized by segmental motions of the nucleic acid components, while the average dipole orientations were favorable for FRET within the complementary complexes.[28] First, novel donor FRET M^2 displayed higher J compared with M^1, although the R_0 values and distance dependence of E were similar for the two monomers (J ~5.2×10^{-14} cm^6 mmol^{-1} vs. 3.2×10^{-14} cm^6 mmol^{-1} for M^2 and M^1, respectively; R_0 ~20 Å; see Materials and Methods for calculation details). Being compared with previously studied Cy3–Cy5 FRET pair terminally attached to series of DNA duplexes, overlap integral J was lower for the pairs M^2/M^3–M^4, which is most likely caused by distinctive spectral properties of the PAH dyes (J ~7.2×10^{-13} cm^6 mmol^{-1} for Cy3–Cy5).[45]

Second, dependence of the FRET efficiency values E on the distance between the donor and acceptor FRET was studied using a series of DNA/RNA targets complementary to **ON1**–**ON4**

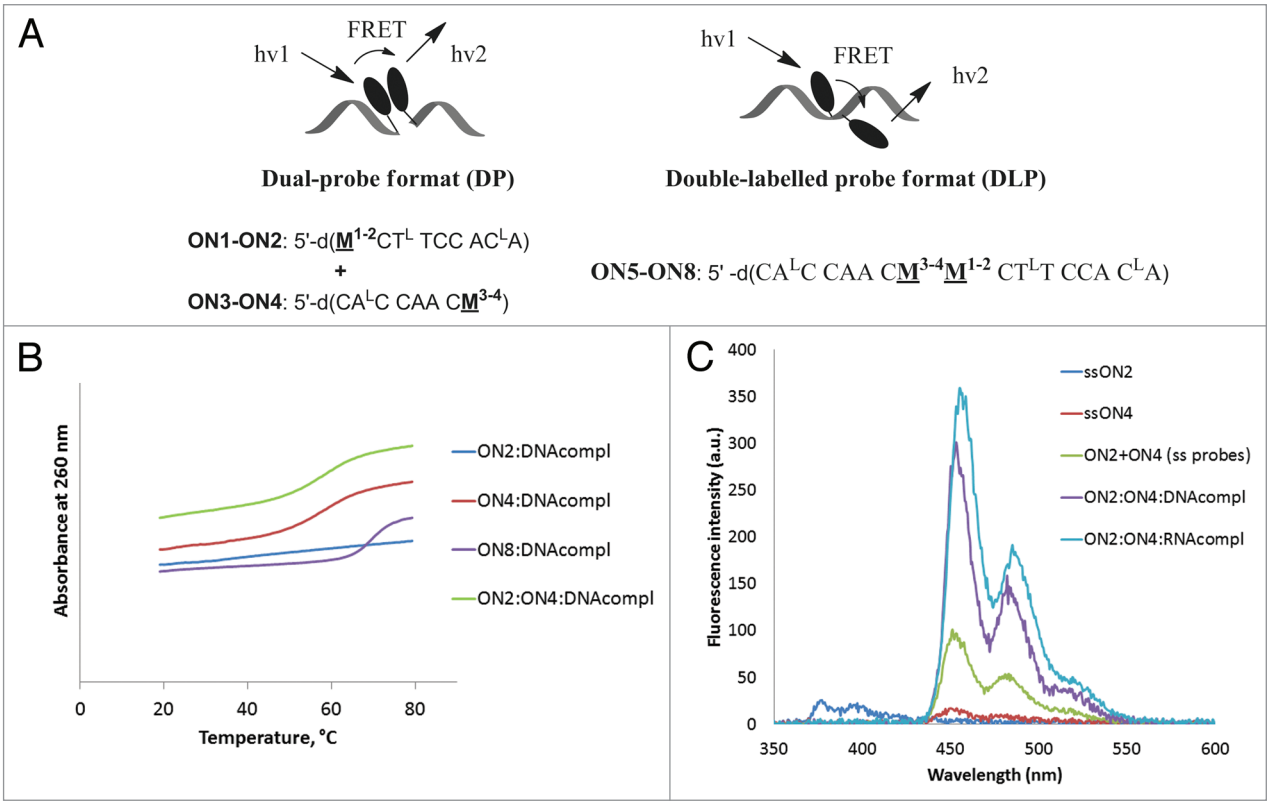

Figure 2. Representation of fluorescent probes prepared in this study (**A**), thermal denaturation curves (**B**), and steady-state fluorescence emission spectra (**C**) of single-stranded model probes **ON2**, **ON4** and their complexes with cDNA and RNA obtained in a medium salt phosphate buffer ([Na^+] = 110 mM) using absorbance at 260 nm (**B**), excitation wavelength 340 nm (**C**) and 1.0 μM concentration of oligonucleotides.

and containing increasing number of separating nucleotides dT_n (rU_n) between the modified monomers (n = 0–9; **Fig. 3A**).[44] Taking length of one nucleotide unit 3.5 Å,[46] the single-stranded gap model allowed measurements of FRET efficiency when the distance between the modified monomers upon hybridization of **ON1**–**ON4** to the targets varied from zero to 31.5 Å (**Fig. 3B**). This assay format was applied because of small Förster distance of the pyrene–perylene FRET pair,[44] although the single-stranded gap model could not disclose orientation dependence of FRET pairs M^2/M^3–M^4 within long double-stranded complexes.[45] Having annealed the FRET probes to the series of DNA/RNA targets and having measured the FRET efficiency values *E* of the resulting complexes as described above, the resulting *E* values were plotted against the distance between the monomers M^1–M^2 and M^3–M^4 (**Fig. 3C and D**). Importantly, the FRET process in the new pairs M^2/M^3–M^4 was inversely proportional to the sixth power of the distance between donor and acceptor, which was of stronger magnitude for DNA targets compared with RNA and in all the cases was in agreement with classic FRET theory (**Fig. 3C and D**).[28]

Molecular models of the complementary and singly-mismatched complexes containing M^1–M^4 showed distance changes *r* = 2–4 Å between the donors and acceptors FRET in presence of mismatch, which is too small in order to decrease the FRET efficiency as indicated by the *E*–*r* plots (**Figs. 3 and 4**). Moreover, molecular modeling showed closer positioning of the M^2

Table 2. Spectral properties of selected model fluorescence probes and their duplexes with cDNA/RNA targets[a]

Probe:target	λ^{abs}_{max}, nm	λ^{fl}_{max}, nm	*E*	Φ_f	FB*
ON1+**ON3**	334,349,426,451	370,422,449,478	0.82	0.05	2.4
ON1:**ON3**:DNA	334,349,428,453	368,422,449,476	1.00	0.05	2.8
ON1:**ON3**:RNA	334,349,429,454	366,420,447,475	1.00	0.05	2.8
ON1+**ON4**	334,349,425,451	370,422,449,478	0.82	0.05	2.2
ON1:**ON4**:DNA	334,349,427,453	368,422,446,477	1.00	0.07	3.1
ON1:**ON4**:RNA	334,349,426,452	366,420,448,478	1.00	0.06	2.9
ON2+**ON4**	330,342,425,451	370,391,449,478	0.86	0.04	2.4
ON2:**ON4**:DNA	330,341,427,452	373,392,448,478	1.00	0.18	21.0
ON2:**ON4**:RNA	330,342,426,452	371,391,446,476	1.00	0.15	18.0
ON8	330,342,425,451	422,449	1.00	0.72	26.0
ON8:DNA	330,341,425,452	420,445	1.00	0.95	44.0
ON8:RNA	330,342,425,453	419,444	1.00	1.00	52.0

[a]Complementary DNA: 5'-d(TGTGGAAGAA GTTGGTG)-3'; complementary RNA: 5'-r(UGUGGAAGAA GUUGGUG)-3'; λ^{abs}_{max}, λ^{fl}_{max}, *E*, Φ_f and FB are absorbance, fluorescence emission maxima, FRET efficiency, fluorescence quantum yield and fluorescence brightness, respectively. *FB = $\Phi_f \times \varepsilon_{max}$, where ε_{max} = maximum molar extinction coefficient of the corresponding probe.

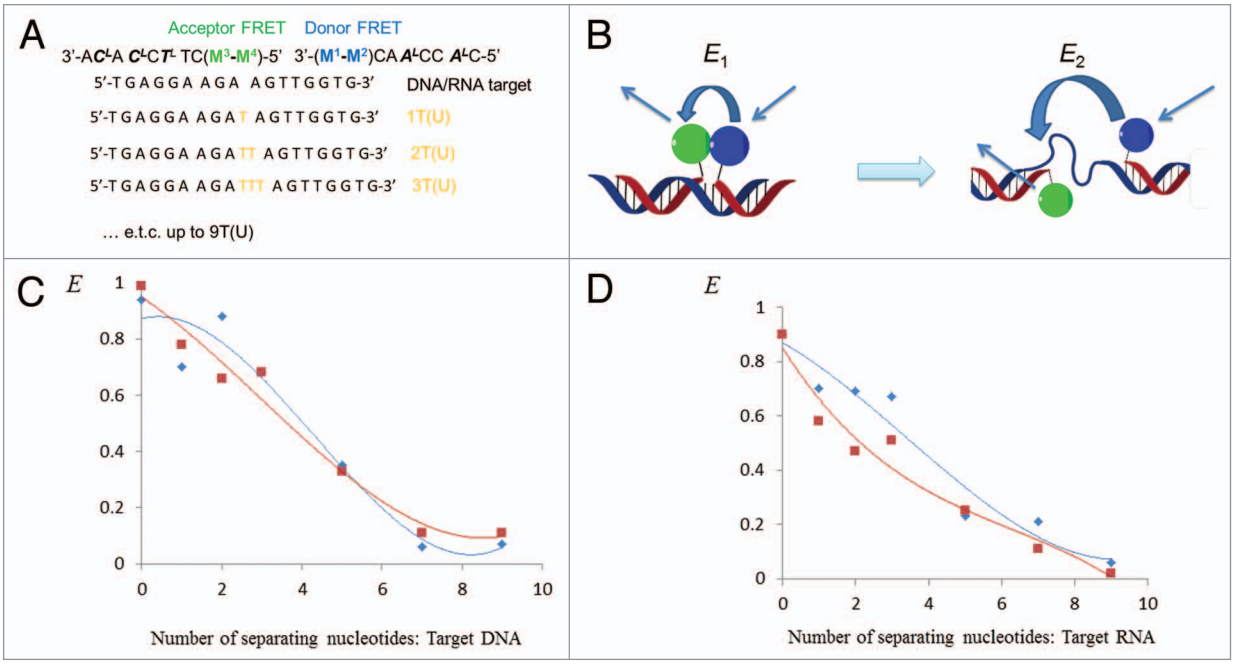

Figure 3. Dependence of FRET efficiency *E* on distance between donor and acceptor FRET. Probes **ON1** + **ON4** and **ON2** + **ON4** (FRET pairs **M¹/M⁴** and **M²/M⁴**) are shown as blue and red lines, respectively. The data presented was obtained assuming *E* = 1.0 for duplexes with target DNA/RNA at n = 0.

within the minor groove compared with isomeric monomer **M¹**, and revealed changes in pyrene orientation in the presence of a mismatch opposite to the pyrene-4-yl monomer **M²** (**Fig. 4C and D** compared with **Fig. 4A and B**). This is to the best of our knowledge the first example of dipole–dipole orientation change between donor and acceptor FRET observed in presence of a single-nucleotide mismatch in a nucleic acid target.[27] Notably, improvement of pyrene's properties as donor FRET was achieved by changing position of the substitution from 1 to 4, which underlines a very strong dependence of the pyrene's spectral properties on the fluorophore's symmetry and adoption within the nucleic acid complexes. Finally, molecular modeling indicated partial positioning of perylene within minor groove of the duplexes accompanied by exposure of the fluorophore into the medium, in all cases with minor interactions between perylene and nucleobases (**Fig. 4**). Such positioning of acceptor FRET is most likely one of the most important factors for obtaining high fluorescence quantum yields of the prepared probes upon binding DNA/RNA targets, since fluorescence response of PAH monitored during the assay is not quenched by the surrounding nucleobases.[28]

Detection of SNP in PCR fragments is a promising method for rapid genotyping in absence of sequencing and microarray equipment.[25] In this study we aimed to develop a homogeneous fluorescence assay for SNP analysis in the clinically important HIV-1 gene fragment encoding protease (HIV *Pol*) using novel **M²/M³–M⁴** FRET pairs (**Fig. 1**). We furthermore aimed at creating a fluorescence assay which could be further applied in e.g., real-time imaging of viral RNA/cDNA and quantative multiplex PCR assays. Initially, a panel of 200 plasma samples obtained from patients currently receiving complex HIV-1/AIDS antiviral therapy at the Russian Federal AIDS Centre was analyzed. We subsequently isolated the total RNA from the plasma samples followed by RT-PCR and Nested PCR amplification rounds using specific primers for the 570 nucleotide *Pol* fragment.[29] The resulting PCR products were purified and sequenced (**Fig. 5**; **Fig. S4**). Having analyzed the resulting sequences, we concluded that within region 2332–2354 mutation G2340A causing resistance of HIV-1 to protease inhibitor (PI) virasept (nelfinavire) is most often accompanied by one or two polymorphisms located three to four nucleotides apart from position 2340. Moreover, the region 2332–2354 often contains mutation G2346A causing resistance of HIV-1 to all PIs available to date (**Table S8**).[47] We obtained model targets (cDNA and RNA variants) corresponding to the sequenced *Pol* regions 2332–2354 from commercial suppliers. In order to evaluate selectivity of target binding, highly polymorphic targets not observed in screening were obtained as well. Finally, we isolated six 570 nt long *Pol* cDNA and characterized them by sequencing (**Fig. 5** and the **Supplemental Material**).

Probes **ON9–ON14** were designed for detection of G2340A and G2346A so the fluorescence enhancing signal of full complementarity corresponded to mutations G2340A and G2346A (**Fig. 5**; preparation and characterization of **ON9–ON14** is described in the **Supplemental Material**). The probes **ON9–ON14** showed binding to the model 2332–2354 targets[29] **T1–T20** at the temperature of fluorescence measurements (19°C; T_m data not shown). On the other hand, **ON9–ON14** did not bind to highly polymorphic sequences **T21–T22**, which proves their selectivity to the complementary *Pol* region 2332–2354. Next, fluorescence studies using model targets **T1–T20** allowed evaluation of mutation sensing by the probes **ON9–ON14** and their characterization with limit of target detection (LOD) values (**Table 3**). Thus, fluorescence

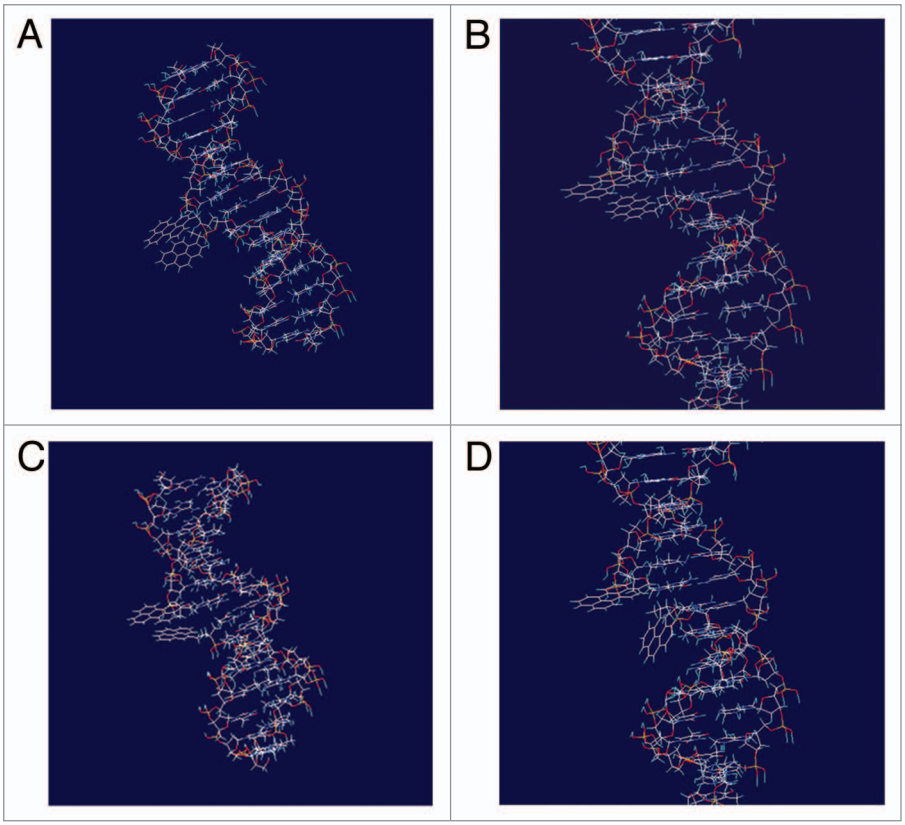

Figure 4. Low-energy structures of complementary and single-mismatched duplexes containing FRET pairs **M¹/M⁴** and **M²/M⁴**: (**A**) **M¹/M⁴** pair within fully matched complex **ON1**:**ON4**:DNA; (**B**) **M¹/M⁴** pair within complex containing mismatch opposite to monomer **M¹** (**ON1**:**ON4**:dmA(8)T); (**C**) **M²/M⁴** pair within fully matched complex **ON2**:**ON4**:DNA; (**D**) **M²/M⁴** pair within complex containing mismatch opposite to monomer **M²** (**ON2**:**ON4**:dmA(8)T).

sensing by dual-probe systems **ON10**+**ON13** and **ON10**+**ON14** was quite similar with higher fluorescence quantum yield for the latter system (data not shown). Interestingly, we observed difference in sensing cDNA and RNA targets, although in both cases all the genotypes were efficiently analyzed, also in the presence of additional polymorphic sequence variations (**Fig. 5**; **Table 3**). The LOD values for **ON9–ON14** were < 5–10 nM which is comparable and in some cases superior to e.g., widely applied molecular beacons and is sufficient for direct sensing of long PCR fragments.[48,49] Finally, annealing of the six purified cDNA fragments with the probe mixtures **ON10**+**ON14**, **ON9**+**ON12** and **ON9**+**ON11** (ss1–ss3) in three analytical tubes was followed by fluorescence measurements and calculation of ratiometric parameter I_{455}/I_{373} (1–3) (**Fig. 5**; see Patients, Materials and Methods section for detailed description of the assay). As can be seen, the performed fluorescence assay allowed rapid and accurate detection of all the six genotypes within the region of interest *Pol* in full agreement with the previously obtained sequencing data (**Fig. 5 and Supplemental Material**).

Discussion

Based on our data, attachment of pyrene in position 4 to 2'-amino-LNA remarkably improved its spectral and photophysical properties compared with the usually applied pyrene-1-yl substituent, also with respect to FRET properties as donor to perylene within nucleic acid complexes. Moreover, fluorescence quantum yield within complementary complexes with DNA/RNA and spectral overlap with perylene were increased for pyrene-4-yl fluorophore compared with the pyrene-1-yl isomer, although the single-stranded probes were quenched by the interactions with polar media in both cases. Changes in dipole–dipole orientation between the pyrene-4-yl and perylene LNA monomers within a dual-probe format allowed rapid and accurate SNP genotyping in cDNA and RNA with a sensitivity lower than 5 nM. This is an important result for the future design of FRET nucleic acid probes for SNP genotyping. Clearly, synthesis of novel pyrene derivatives is a promising strategy for development of novel effective biosensors, as the distinctive advantage of PAH fluorophores in contrast to e.g., cyanines and xanthenes is their high photo- and chemical stability. Together with large Stokes shift (115 nm), target binding affinity and selectivity, pyrene–perylene LNA/DNA FRET probes described herein provide great potential for the development of nucleic acid based biosensors for imaging and clinical diagnostics.

Patients, Materials and Methods

Phosphoramidite reagents **5**,[41] **6**[42] and **9**[43] were synthesized following published procedures; phosphoramidite reagent **3** was prepared as described below. Pyrene-1- and pyrene-4-carbaldehydes were obtained from commercial suppliers (Sigma-Aldrich, cat. no. 144037, and Achemica Corp., custom synthesis, respectively). 9,10-Diphenylantracene (DPA), 1-pyrenebutyric acid and perylene used in spectral studies were recrystallized. HPLC grade light petroleum ether, 1,2-dichloroethane, *n*-hexane and ethyl acetate were distilled and stored over activated 4 Å molecular sieves. DCM was distilled over CaH_2. All other reagents and solvents obtained from commercial suppliers were used as received. Photochemical studies were performed using spectroquality cyclohexane and methanol.

NMR spectra were recorded at 303 K on Varian Gemini 2000 300 MHz instrument. Chemical shifts are reported in ppm relative to solvents peaks ($CDCl_3$: 7.26 ppm for ^1H and 77.0 ppm for ^{13}C; 85% aq. H_3PO_4: 0.00 ppm for ^{31}P). ^1H NMR coupling constants are reported in Hz and refer to apparent multiplicities. High resolution MALDI mass spectra were recorded in positive ion mode using an IonSpec Fourier Transform ICR mass spectrometer. Analytical thin-layer chromatography was performed

on Kieselgel 60 F_{254} precoated aluminum plates (Merck). Silica gel column chromatography was performed using Merck Kieselgel 60 0.040–0.063 mm.

Unmodified DNA/RNA strands were obtained from commercial suppliers and used without further purification. Oligonucleotide synthesis of the fluorescent probes used in this study was performed on a PerSpective Biosystems Expedite 8909 instrument in 200 nmol scale using manufacturer's standard protocols. For incorporation of monomers **M**[1]–**M**[4] a hand-coupling procedure was applied (25 min coupling). The coupling efficiencies of standard DNA phosphoramidites and reagents **3**, **5**–**6** and **9** based on the absorbance of the dimethoxytrityl cation released after each coupling varied between 92% and 100%. Cleavage from solid support and removal of nucleobase protecting groups was performed using 32% aqueous ammonia and methylamine 1:1, v/v, for 4 h at room temperature (5'-terminal and internally labeled probes). In case of 3'-modified probes, a universal support 40 (GE Healthcare) was used. Cleavage from the latter and removal of nucleobase protecting groups was performed using 4 M ammonia in abs. MeOH (1 h, rt), followed by addition of 32% aqueous ammonia (6 h, 55°C). The product oligonucleotides were purified by DMT-ON reverse-phase (RP) HPLC using the Waters System 600 equipped with Xterra MS C18-column (5 μm, 150 mm × 7.8 mm). Elution was performed starting with an isocratic hold of A-buffer for 5 min followed by a linear gradient to 70% B-buffer over 40 min at a flow rate of 1.0 mL/min (A-buffer: 0.05 M triethyl ammonium acetate, pH 7.4; B-buffer: 25% buffer A, 75% CH_3CN). RP purification was followed by detritylation (80% aq. AcOH, 20 min), precipitation (acetone, –18°C, 12 h) and washing with acetone three times. The identity and purity of oligonucleotides was then verified by MALDI-TOF mass spectrometry and IE HPLC, respectively. IE HPLC was performed using the Merck Hitachi LaChrom instrument equipped with Dionex DNAPac Pa-100 column (250 mm × 4 mm). Elution was performed starting with an isocratic hold of A- and C-buffers for 2 min followed by a linear gradient to 60% B-buffer over 28 min at a flow rate of 1.0 mL/min (A-buffer: MQ water; B-buffer: 1 M $NaClO_4$, C-buffer: 25 mM Tris-Cl, pH 8.0). MALDI-TOF mass spectrometry analysis was performed using a MALDI-LIFT system on the Ultraflex II TOF/TOF instrument from Bruker and using HPA-matrix (10 mg 3-hydroxypicolinic acid, 50 mM ammonium citrate in 70% aqueous acetonitrile).

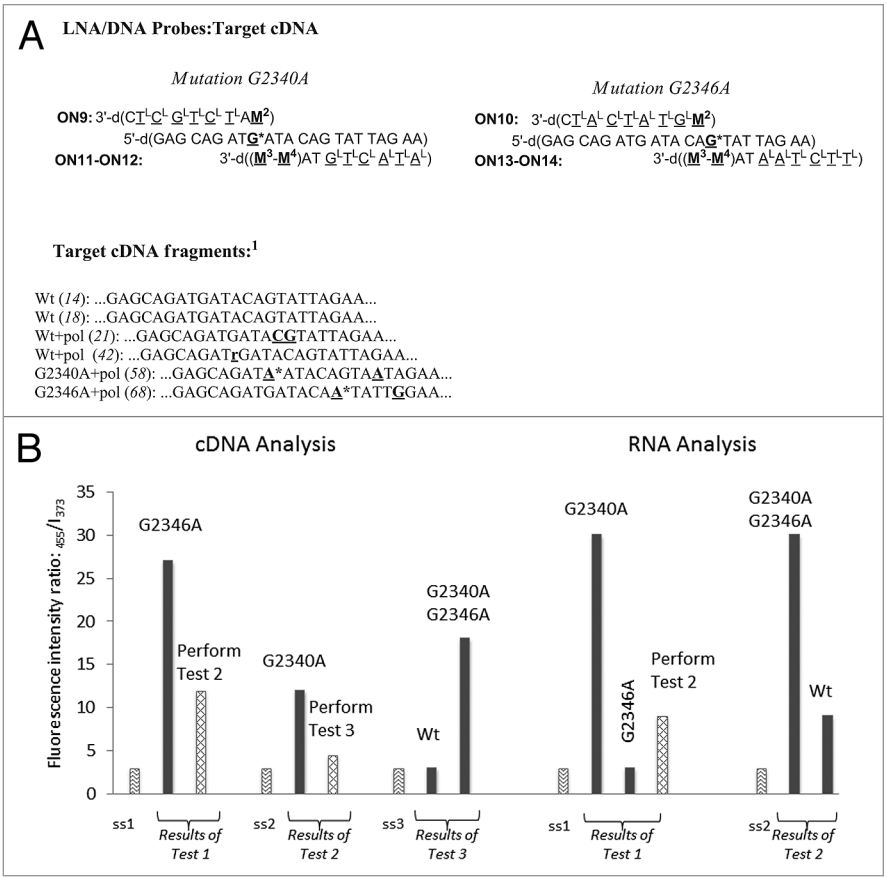

Figure 5. Detection of HIV PR cDNA and RNA fragments. Ss1–ss3 = **ON10** + **ON14**, **ON9** + **ON12** and **ON9** + **ON11**, respectively. The data are presented according to homogeneous fluorescence genotyping assay described in Patients, Material and Methods section. Target abbreviations: Wt, wild type; Wt + pol, wild-type at positions 2340 and 2346 containing polymorphic mutations; G2340A (G2346A) + pol, mutation G→A at position 2340 (2346) and additional polymorphic mutations; r, purine as low-complexity or repetitive element.[1] For complete sequencing data of the cDNA fragments, see the **Supplemental Material**.

Synthesis of modified monomer M[2]. *(1R,3R,4R,7S)-1-(4,4'-Dimethoxytrityloxymethyl)-7-hydroxy-5-(pyren-4-yl)methyl-3-(thymin-1-yl)-2-oxa-5-azabicyclo[2.2.1]heptane (2).* Reductive alkylation of nucleoside **1** (470 mg, 1 mmol) was performed with pyrene-4-carbaldehyde (230 mg, 1 mmol) in the presence of $NaBH(OAc)_3$ (320 mg, 1.5 mmol) in 1,2-dichloromethane (15 mL) at rt for 12 h. A mixture of absolute EtOH with toluene and Et_3N (9:9:2, v/v/v) was then added, and the resulting mixture was evaporated to dryness under reduced pressure. The residue obtained was purified by column chromatography (55→60% EtOAc in a light petroleum ether, v/v) to afford nucleoside **2** as a white solid material (560 mg, 87%). ^{1}H NMR ($CDCl_3$) δ 9.25 (br s, 1H, NH), 8.36 (d, J = 7.9 Hz, 1H), 8.14–8.10 (m, 3H), 8.05 (s, 1H), 8.00–7.91 (m, 4H), 7.70 (s, 1H, H6), 7.46–7.43 (m, 2H), 7.34–7.20 (m, 7H), 6.80 (dd, J = 2.1 and 8.8 Hz, 4H), 6.10 (s, 1H, H1'), 4.77 (d, J = 13.4 Hz, 1H, CH_2-pyrene), 4.50 (d, J = 13.3 Hz, 1H, CH_2-pyrene), 4.26 (s, 1H, H3'), 3.75 (s, 6H, 2 × OCH_3), 3.72 (s, 1H, H2'), 3.38 (d, J = 11.5 Hz, 1H, H5'a), 3.34 (d, J = 12.8 Hz, 1H, H5'b), 2.95 (d, J = 10.0 Hz, 1H, H5''a), 2.65 (d, J = 10.0 Hz, 1H, H5''b), 1.72 (s, 3H, 5-CH_3); ^{13}C NMR ($CDCl_3$) δ 164.1 (C4), 158.7, 150.1 (C2), 144.6, 135.7, 135.5, 135.2, 132.7, 131.6, 131.0, 130.6, 130.2, 130.1, 128.2, 128.1, 128.0, 127.6, 127.3, 127.1, 126.1, 125.9, 125.4, 125.2, 124.4,

Table 3. Detection of mutations G2340A and G2346A in cDNA/RNA targets using FRET LNA/DNA probes **ON9–ON14**[a]

Probes	Target	Fluorescence sensing of binding HIV-1 *Pol* (target abbreviation)	LOD, nM
ON9 + **ON11**	cDNA	6-fold increased emission (G2340A + G2346A + pol)	10
ON9 + **ON12**	cDNA	4-fold increased emission (G2340A + pol)	10
ON10 + **ON14**	cDNA	9-fold increased emission (G2346A + pol)	5
ON9 + **ON12**	RNA	10-fold increased emission (G2340A + pol) No light-up (G2346A + pol)	< 5
ON10 + **ON14**	RNA	10-fold increased emission (G2340A + G2346A + pol)	< 5

[a]G2340A (G2346A), mutation G→A at position 2340 (2346); pol, polymorphic mutation(s); LOD, limit of target detection.

121.4, 113.3, 110.4 (C5), 88.9 (C4'), 86.6 (CAr_3), 82.6 (C1'), 70.8 (C3'), 66.7 (C5'), 59.7 (C2'), 56.4 (CH_2-pyrene), 55.3 (2 × OCH_3), 53.7 (C5''), 12.7 (5-CH_3); MALDI-HRMS: *m/z* 808.2992 ([M + Na]$^+$, $C_{49}H_{43}N_3O_7Na^+$ calcd 808.2999).

(1R,3R,4R,7S)-7-(2-Cyanoethoxy(diisopropylamino) phosphinoxy)-1-(4,4'-dimethoxytrityloxymethyl)-5-(pyren-4-yl) methyl-3-(thymin-1-yl)-2-oxa-5-azabicyclo[2.2.1]heptane (3). 2-Cyanoethyl *N,N*-diisopropylphosphoramidochloridite (250 mg, 1 mmol) was added dropwise to a stirred solution of nucleoside **2** (550 mg, 0.7 mmol) and *N,N*-(diisopropyl)ethylamine (DIPEA, 2.5 mL) in DCM (10 mL). After stirring for 12 h at rt, the reaction mixture was diluted with DCM and the resulting mixture was washed with sat. aq. $NaHCO_3$, dried (Na_2SO_4) and evaporated to dryness under reduced pressure. The residue obtained was purified by column chromatography (50–55% EtOAc in *n*-hexane, v/v) to afford phosphoramidite **3** as a white foam (630 mg, 91%). ^{31}P NMR ($CDCl_3$) δ 149.6, 149.4; MALDI-HRMS: *m/z* 1008.4065 ([M+Na]$^+$, $C_{58}H_{60}N_5O_8PNa^+$ calcd 1008.4072).

UV-visible absorbance spectra and thermal denaturation experiments. UV-visible absorbance spectra and thermal denaturation experiments were performed on a Perkin Elmer Lambda 35 UV/VIS Spectrometer equipped with PTP 6 (Peltier Temperature Programmer) in a medium salt phosphate buffer (100 mM NaCl, 10 mM Na-phosphate, 0.1 mM EDTA, pH 7.0). Concentrations of oligonucleotides were calculated using the following extinction coefficients (OD_{260}/μmol): G, 10.5; A, 13.9; T/U, 7.9; C, 6.6; **M**[1] 20.2; **M**[2], 16.9; **M**[3]–**M**[4], 33.2. For determination of the extinction coefficient of pyrene-4-ylmethyl modification, a solution of pyrene-4-carbaldehyde in 0.5% DMSO–water was used. Oligonucleotides (1.0 μM each strand) were thoroughly mixed, denatured by heat (5 min at 85°C) and subsequently cooled to the starting temperature of experiment. Thermal denaturation temperatures (T_m values, °C) were determined as the maximum of the first derivative of the thermal denaturation curve at the corresponding wavelength (*A* vs. temperature). Reported T_m values are averages of at least two measurements with resulting T_m within ± 0.5°C.

Fluorescence spectra. Fluorescence spectra were recorded in a medium salt phosphate buffer described above on a PerkinElmer LS 55 luminescence spectrometer equipped with a Peltier temperature controller using an excitation wavelength of 340 nm, excitation slit of 4.0 nm, emission slit of 2.5 nm, scan speed of 120 nm/min and 0.25–1.0 μM concentrations of the single-stranded probe or the corresponding complementary complex.

The fluorescence quantum yields. The fluorescence quantum yields (Φ_f) were measured by the relative method[28,29] using standards of highly diluted solutions of 1-pyrenebutyric acid (Φ_f = 0.07) in methanol, perylene (Φ_f = 0.93) and 9,10-diphenylantracene (Φ_f = 0.95) in cyclohexane. The samples used in quantum yield measurements were not degassed; concentrations were 0.25 μM. Excitation spectra were obtained using emission wavelength at 510 nm.

Discrimination factor. Discrimination factor (DF) values[50] were determined as a ratio of fluorescent signal (fluorescence intensity or fluorescence intensity ratio) at corresponding λ^{fl} of fully-matched duplex to single-base mismatched one. DF > 1 = quenching of fluorescence at corresponding λ^{fl}; DF < 1 = fluorescence light-up.

FRET efficiency values. FRET efficiency values *E* for pyrene-perylene FRET pairs were calculated using equiation:[35] $E = \varepsilon_A/\varepsilon_D \times (I_{AD}/I_A - 1)$, where ε_A and ε_D are the molar extinction coefficients of the acceptor and donor at the excitation wavelength, and I_{AD} and I_A are the fluorescence intensities at the acceptor emission wavelength in the presence and absence of the donor, respectively.

Limit of target detection (LOD) values. Limit of target detection (LOD) values were determined by series of dilution experiments following previously described protocol.[29] Relevant fluorescent oligonucleotides at concentrations 500, 250, 100, 50, 20, 10, 5, and 1 nM were mixed in a medium salt phosphate buffer in molar ratios described above. Upon annealing, a fluorescence signal was measured at λ^{fl} 455 nm. LOD value of each complex was then defined as a lowest complex concentration such that the fluorescence signal to noice ratio (S/N) relative to the blank solution of a medium salt phosphate buffer was minimum three.

Förster distances. Förster distances R_0 were determined using Förster Energy Transfer module of PhotochemCAD ver. 2.0 software[51] and using the following equations:[44]

$$R_0 = (8.79 \times 10^{-5}\, J\, \phi_D\, n^{-4}\, \kappa^2)^{-1/6} \text{ (in Å)} \quad (1)$$

$$J = \int \varepsilon_A(\lambda)\, f_D(\lambda)\, \lambda^4\, d\lambda / \int f_D(\lambda)\, \lambda^4 \text{ (in cm}^6\text{ mmol}^{-1}\text{)} \quad (2)$$

where *J* is the normalized spectral overlap of the donor emission spectrum and the acceptor absorption spectrum, ϕ_D is the quantum yield for donor emission in absence of the acceptor, *n* is the refractive index of the solution, κ^2 is an orientation factor depending on the relative orientation of the emission dipole of the donor and the excitation dipole of the acceptor, $\varepsilon_A(\lambda)$ is the extinction coefficient of the acceptor ($M^{-1}cm^{-1}$) and $f_D(\lambda)$ is the corrected emission spectrum of the donor per unit wavelength

interval. Steady-state fluorescence emission and absorbance spectra of the corresponding complementary oligonucleotides containing donor and acceptor FRET were uploaded into the PhotochemCAD database, as well as FRET efficiency and distance D–A values estimated by fluorescence measurements and molecular modeling described below, respectively. Resulting values using κ^2 value of 2/3 (lit.[44]): R_0 = 19.8 Å, $J = 3.21 \times 10^{-14}$ cm^6 mmol^{-1}, pair **M**^{1}/**M**^{3}; R_0 = 20.1 Å, $J = 3.20 \times 10^{-14}$ cm^6 mmol^{-1}, pair **M**^{1}/**M**^{4}; R_0 = 21.9 Å, $J = 5.08 \times 10^{-14}$ cm^6 mmol^{-1}, pair **M**^{1}/**M**^{3}; R_0 = 21.5 Å, $J = 5.2 \times 10^{-14}$ cm^6 mmol^{-1}, pair **M**^{1}/**M**^{4}. Reference values for pyrene–perylene FRET pair in cyclohexane: R_0 = 31.3 Å, $J = 2.3 \times 10^{-14}$ cm^6 mmol^{-1} (2.4×10^{-14} cm^6 mmol^{-1}, lit.[44]).

Molecular modeling. Nucleic acid duplexes were built in B-type helical geometry using Chem3D Pro 12.0 for incorporation of fluorophores and further analyzed by MacroModel V9.1.[52] When doing this the structures were minimized using the Polak–Ribiere conjugate gradient method, the all-atom AMBER force field,[53] and GB/SA solvation model[54] as implemented in MacroModel V9.1. Non-bonded interactions were treated with extended cut-offs (van der Waals 8.0 Å and electrostatics 20.0 Å).

Isolation of total HIV RNA. From the 200 plasma samples followed by RT-PCR and NESTED-PCR amplification were performed using in-house testing system "Amplisense® HIV-genotype-EPh" obtained from Central Institute of Epidemiology and PCR amplifier GeneAmp PCR System 2400. Selected patients currently receive combined anti-HIV/AIDS therapy; the negative controls included HIV-negative serum samples and MQ water. Purification of the cDNA products was performed by enzymatic method using ExoSAP-IT® on PCR amplifier GeneAmp PCR System 2400, followed by detection of 570 nucleotides long HIV-1 protease cDNA fragments in 1% agarose gel. Additionally, cDNA fragments from six different patients' samples were analyzed using standard clinical test "Amplisense® HIV-genotype-EPh" for 1,302 nt protease and reverse transcriptase gene fragments. Afterwards, five PCR amplification reactions were performed for each clinical sample. The collected single-stranded cDNA were purified as described above; yield of the resulting 570 nt fragments estimated by measuring OD_{260} was approx. 0.1 nmol (0.4–0.6 mg).

Dye terminator cycle sequencing of the PCR products. Dye terminator cycle sequencing of the PCR products was performed following standard clinical genotyping protocol in an automatic Beckman CEQ2000XL sequenator using GenomeLabTM DTCS Quick Start Kit (Beckman Coulter). Sequencing results interpretation was performed using Stanford Hospital and Clinics HIVdb Program available on the internet.

Homogeneous fluorescence assay for SNP analysis of HIV-1 Pol cDNA using ON9–ON14. In separate vials the purified cDNA fragment (10 μL of 1.0 μM stock solutions) and water (negative control) were mixed with the probes ss1–ss3 (25 μL of 1.0 μM stock solution; ss1: **ON10** and **ON14**; ss2: **ON9** and **ON12**; ss3: **ON9** and **ON11**) in DNA hybridization buffer (medium salt PBS containing 10 mM EDTA and 0.1% Tween 20). The vials were marked as "test 1–3" for the mixtures of cDNA with ss1–ss3, respectively; the corresponding negative controls were marked "0." The resulting samples were annealed at 85°C for 5 min followed by cooling to rt over 1 h. Fluorescence measurements were performed using excitation wavelength of 340 nm, and monitoring emission at 455 nm and 373 nm. Fluorescence response was analyzed using the following ratiometric equations:

Test 1: I_{455}/I_{373} (test 1)/I_{455}/I_{373} (0) = 9.0→mutation G2346A; I_{455}/I_{373} (test 1)/I_{455}/I_{373} (0) = 4.0→analysis of test 2.

Test 2: I_{455}/I_{373} (test 2)/I_{455}/I_{373} (0) = 4.0→mutation G2340A; I_{455}/I_{373} (test 2)/I_{455}/I_{373} (0) = 1.5→analysis of test 3.

Test 3: I_{455}/I_{373} (test 3)/I_{455}/I_{373} (0) = 1.0→wild type target at both positions 2340 and 2346; I_{455}/I_{373} (test 3)/I_{455}/I_{373} (0) = 6.0→both mutations G2340A and G2346A are present.

Homogeneous fluorescence assay for SNP analysis of HIV-1 Pol RNA using ON9–ON10, ON12 and ON14. In separate vials the RNA target (10 μL of 1.0 μM stock solutions) and water (negative control) were mixed with the probes ss1–ss2 (25 μL of 1.0 μM stock solution; ss1: **ON9** and **ON12**; ss2: **ON10** and **ON14**) in DNA hybridization buffer described above. The vials were marked as "test 1–2" for the mixtures of RNA with ss1–ss2, respectively; the corresponding negative controls were marked "0." The resulting samples were annealed at 85°C for 5 min followed by cooling to rt over 1 h. Fluorescence measurements were performed using excitation wavelength of 340 nm, and monitoring emission at 455 nm and 373 nm. Fluorescence response was analyzed using the following ratiometric equations:

Test 1: I_{455}/I_{373} (test 1)/I_{455}/I_{373} (0) = 10.0→mutation G2340A; I_{455}/I_{373} (test 1)/I_{455}/I_{373} (0) = 1.0→mutation G2346A; I_{455}/I_{373} (test 1)/I_{455}/I_{373} (0) = 3.0→analysis of test 2

Test 2: I_{455}/I_{373} (test 2)/I_{455}/I_{373} (0) = 10.0→both mutations G2340A and G2346A are present; I_{455}/I_{373} (test 2)/I_{455}/I_{373} (0) = 3.0→wild type target at both positions 2340 and 2346.

Disclosure of Potential Conflicts of Interest

No potential conflicts of interest were disclosed.

Acknowledgments

The authors acknowledge financial support from The Villum Foundation and The Sapere Aude program of The Danish Council for Independent Research.

Supplemental Materials

Supplemental materials may be found here:
www.landesbioscience.com/journals/artificialdna/article/25903

References

1. Hupfeld J, Efferth T. Review. Drug resistance of human immunodeficiency virus and overcoming it by natural products. In Vivo 2009; 23:1-6; PMID:19368117
2. Holmes EC. Virology. Helping the resistance. Science 2010; 328:1243-4; PMID:20522766; http://dx.doi.org/10.1126/science.1190994
3. Mehellou Y, De Clercq E. Twenty-six years of anti-HIV drug discovery: where do we stand and where do we go? J Med Chem 2010; 53:521-38; PMID:19785437; http://dx.doi.org/10.1021/jm900492g
4. Twyman RM. Encyclopedia of Diagnostic Genomics and Proteomics, Marcel Dekkar Inc., New York, 2005:1202.
5. Costabile M, Quach A, Ferrante A. Molecular approaches in the diagnosis of primary immunodeficiency diseases. Hum Mutat 2006; 27:1163-73; PMID:16960849; http://dx.doi.org/10.1002/humu.20412
6. Chen X, Kwok PY. Template-directed dye-terminator incorporation (TDI) assay: a homogeneous DNA diagnostic method based on fluorescence resonance energy transfer. Nucleic Acids Res 1997; 25:347-53; PMID:9016564; http://dx.doi.org/10.1093/nar/25.2.347
7. Nazarenko IA, Bhatnagar SK, Hohman RJ. A closed tube format for amplification and detection of DNA based on energy transfer. Nucleic Acids Res 1997; 25:2516-21; PMID:9171107; http://dx.doi.org/10.1093/nar/25.12.2516
8. Lopez-Crapez E, Bazin H, Andre E, Noletti J, Grenier J, Mathis G. A homogeneous europium cryptate-based assay for the diagnosis of mutations by time-resolved fluorescence resonance energy transfer. Nucleic Acids Res 2001; 29:E70; PMID:11452039; http://dx.doi.org/10.1093/nar/29.14.e70
9. Bengra C, Mifflin TE, Khripin Y, Manunta P, Williams SM, Jose PA, et al. Genotyping of essential hypertension single-nucleotide polymorphisms by a homogeneous PCR method with universal energy transfer primers. Clin Chem 2002; 48:2131-40; PMID:12446468
10. Jares-Erijman EA, Jovin TM. FRET imaging. Nat Biotechnol 2003; 21:1387-95; PMID:14595367; http://dx.doi.org/10.1038/nbt896
11. Xiao M, Kwok PY. DNA analysis by fluorescence quenching detection. Genome Res 2003; 13:932-9; PMID:12727909; http://dx.doi.org/10.1101/gr.987803
12. Asseline U. Development and applications of fluorescent oligonucleotides. Curr Org Chem 2006; 10:491-518; http://dx.doi.org/10.2174/138527206776055349
13. Roy R, Hohng S, Ha T. A practical guide to single-molecule FRET. Nat Methods 2008; 5:507-16; PMID:18511918; http://dx.doi.org/10.1038/nmeth.1208
14. Malakhov AD, Skorobogatyi MV, Prokhorenko IA, Gontarev SV, Kozhich DT, Stetsenko DA, et al. 1-(Phenylethynyl)pyrene and 9,10-bis(phenylethynyl) anthracene, useful fluorescent dyes for DNA labeling: Excimer formation and energy transfer. Eur J Org Chem 2004; 6:1298-307; http://dx.doi.org/10.1002/ejoc.200300677
15. Skorobogatyj MV, Pchelintseva AA, Ustinov AV, Korshun VA, Malakhov AD. Perylene attached to DNA through stiff or flexible linker: duplex stability and FRET. Nucleosides Nucleotides Nucleic Acids 2005; 24:931-4; PMID:16248065; http://dx.doi.org/10.1081/NCN-200059283
16. Chou CC, Huang YH. Nucleic acid sandwich hybridization assay with quantum dot-induced fluorescence resonance energy transfer for pathogen detection. Sensors (Basel) 2012; 12:16660-72; PMID:23211753; http://dx.doi.org/10.3390/s121216660
17. Astakhova IK, Kumar TS, Campbell MA, Ustinov AV, Korshun VA, Wengel J. Branched DNA nanostructures efficiently stabilised and monitored by novel pyrene-perylene 2'-α-L-amino-LNA FRET pairs. Chem Commun (Camb) 2013; 49:511-3; PMID:23201901; http://dx.doi.org/10.1039/c2cc37547h
18. Preus S, Wilhelmsson LM. Advances in quantitative FRET-based methods for studying nucleic acids. Chembiochem 2012; 13:1990-2001; PMID:22936620; http://dx.doi.org/10.1002/cbic.201200400
19. Freeman R, Girsh J, Jou AF, Ho JA, Hug T, Dernedde J, et al. Optical aptasensors for the analysis of the vascular endothelial growth factor (VEGF). Anal Chem 2012; 84:6192-8; PMID:22746189; http://dx.doi.org/10.1021/ac3011473
20. Whitcombe D, Brownie J, Gillard HL, McKechnie D, Theaker J, Newton CR, et al. A homogeneous fluorescence assay for PCR amplicons: its application to real-time, single-tube genotyping. Clin Chem 1998; 44:918-23; PMID:9590362
21. Whitcombe D, Theaker J, Guy SP, Brown T, Little S. Detection of PCR products using self-probing amplicons and fluorescence. Nat Biotechnol 1999; 17:804-7; PMID:10429248; http://dx.doi.org/10.1038/11751
22. Crockett AO, Wittwer CT. Fluorescein-labeled oligonucleotides for real-time pcr: using the inherent quenching of deoxyguanosine nucleotides. Anal Biochem 2001; 290:89-97; PMID:11180941; http://dx.doi.org/10.1006/abio.2000.4957
23. Vaughn CP, Elenitoba-Johnson KSJ. Hybridization-induced dequenching of fluorescein-labeled oligonucleotides: a novel strategy for PCR detection and genotyping. Am J Pathol 2003; 163:29-35; PMID:12819008; http://dx.doi.org/10.1016/S0002-9440(10)63627-9
24. Ruiz-Ponte C, Carracedo A, Barros F. Duplication and deletion analysis by fluorescent real-time PCR-based genotyping. Clin Chim Acta 2006; 363:138-46; PMID:16153621; http://dx.doi.org/10.1016/j.cccn.2005.05.044
25. Marras SAE, Tyagi S, Kramer FR. Real-time assays with molecular beacons and other fluorescent nucleic acid hybridization probes. Clin Chim Acta 2006; 363:48-60; PMID:16111667; http://dx.doi.org/10.1016/j.cccn.2005.04.037
26. Martinez-Serra J, Gutiérrez A, Marcús TF, Soverini S, Amat JC, Navarro-Palou M, et al. Four-channel asymmetric Real-Time PCR hybridization probe assay: a rapid pre-screening method for critical BCR-ABL kinase domain mutations. Clin Biochem 2012; 45:345-51; PMID:22266405; http://dx.doi.org/10.1016/j.clinbiochem.2011.12.026
27. De Angelis DA, Dino A. Why FRET over genomics? Physiol Genomics 1999; 1:93-9; PMID:11015566
28. Lakowicz JR. Principles of Fluorescence Spectroscopy, 3th Ed., Springer, Singapore, 2006.
29. Astakhova IK, Samokhina E, Babu BR, Wengel J. Novel (phenylethynyl)pyrene-LNA constructs for fluorescence SNP sensing in polymorphic nucleic acid targets. Chembiochem 2012; 13:1509-19; PMID:22761036; http://dx.doi.org/10.1002/cbic.201200079
30. Umemoto T, Hrdlicka PJ, Babu BR, Wengel J. Sensitive SNP dual-probe assays based on pyrene-functionalized 2'-amino-LNA: lessons to be learned. [and references therein]. Chembiochem 2007; 8:2240-8; PMID:17979173; http://dx.doi.org/10.1002/cbic.200700408
31. Kalra N, Babu BR, Parmar VS, Wengel J. Conformationally controlled high-affinity targeting of RNA or DNA by novel 2'-amino-DNA/LNA mixmers and pyrenyl-functionalized 2'-amino-DNA. Org Biomol Chem 2004; 2:2885-7; PMID:15480448; http://dx.doi.org/10.1039/b411626g
32. Filichev VV, Astakhova IV, Malakhov AD, Korshun VA, Pedersen EB. 1-, 2-, and 4-ethynylpyrenes in the structure of twisted intercalating nucleic acids: structure, thermal stability, and fluorescence relationship. Chemistry 2008; 14:9968-80; PMID:18810743; http://dx.doi.org/10.1002/chem.200800380
33. Korshun VA, Malakhov AD, Astakhova IV, Pedersen EB, Filichev VV. DNA glue: 1-, 2- and 4-ethynylpyrenes in the structure of twisted intercalating nucleic acids (TINAs), DNA duplexes/triplexes and interstrand excimer formation. Nucleic Acids Symp Ser 2008; 52:347-8; http://dx.doi.org/10.1093/nass/nrn175
34. Astakhova IV, Korshun VA. 2- and 4-Phenylethynylpyrenes, novel fluorescent labeles for DNA. Russ J Bioorganic Chem 2008; 34:510-2; http://dx.doi.org/10.1134/S1068162008040171
35. Lindegaard D, Madsen AS, Astakhova IV, Malakhov AD, Babu BR, Korshun VA, et al. Pyrene-perylene as a FRET pair coupled to the N2'-functionality of 2'-amino-LNA. Bioorg Med Chem 2008; 16:94-9; PMID:17920888; http://dx.doi.org/10.1016/j.bmc.2007.04.056
36. Kashida H, Takatsu T, Sekiguchi K, Asanuma H. An efficient fluorescence resonance energy transfer (FRET) between pyrene and perylene assembled in a DNA duplex and its potential for discriminating single-base changes. Chemistry 2010; 16:2479-86; PMID:20066689; http://dx.doi.org/10.1002/chem.200902078
37. Singh SK, Kumar R, Wengel J. Synthesis of 2'-amino-LNA: a novel conformationally restricted high-affinity oligonucleotide analogue with a handle. J Org Chem 1998; 63:10035-9; http://dx.doi.org/10.1021/jo9814445
38. Madsen AS, Jørgensen AS, Jensen TB, Wengel J. Large scale synthesis of 2'-amino-LNA thymine and 5-methylcytosine nucleosides. J Org Chem 2012; 77:10718-28; PMID:23145501; http://dx.doi.org/10.1021/jo302036h
39. Baxter EW, Reitz AB. Reductive Aminations of Carbonyl Compounds with Borohydride and Borane Reducing Agents; Organic Reactions, vol. 59, Wiley, New York, 2002.
40. Caruthers MH, Barone AD, Beaucage SL, Dodds DR, Fisher EF, McBride LJ, et al. Chemical synthesis of deoxyoligonucleotides by the phosphoramidite method. Methods Enzymol 1987; 154:287-313; PMID:3431460; http://dx.doi.org/10.1016/0076-6879(87)54081-2
41. Hrdlicka PJ, Babu BR, Sørensen MD, Wengel J. Interstrand communication between 2'-N-(pyren-1-yl)methyl-2'-amino-LNA monomers in nucleic acid duplexes: directional control and signalling of full complementarity. Chem Commun (Camb) 2004; 1478-9; PMID:15216339; http://dx.doi.org/10.1039/b404446k
42. Astakhova IV, Kumar TS, Wengel J. Fluorescent oligonucleotides containing a novel perylene 2'-amino-α-L-LNA: synthesis and analytical potential. Collect Czech Chem Commun 2011; 76:1347-60; http://dx.doi.org/10.1135/cccc2011096
43. Astakhova IV, Korshun VA, Jahn K, Kjems J, Wengel J. Perylene attached to 2'-amino-LNA: synthesis, incorporation into oligonucleotides, and remarkable fluorescence properties in vitro and in cell culture. Bioconjug Chem 2008; 19:1995-2007; PMID:18771303; http://dx.doi.org/10.1021/bc800202v
44. Masuko M, Ohuchi S, Sode K, Ohtani H, Shimadzu A. Fluorescence resonance energy transfer from pyrene to perylene labels for nucleic acid hybridization assays under homogeneous solution conditions. Nucleic Acids Res 2000; 28:E34; PMID:10734211; http://dx.doi.org/10.1093/nar/28.8.e34
45. Iqbal A, Arslan S, Okumus B, Wilson TJ, Giraud G, Norman DG, et al. Orientation dependence in fluorescent energy transfer between Cy3 and Cy5 terminally attached to double-stranded nucleic acids. Proc Natl Acad Sci U S A 2008; 105:11176-81; PMID:18676615; http://dx.doi.org/10.1073/pnas.0801707105
46. Zenger V. Principles of Nucleic Acid Structure, Springer Verlag, 1984.

47. Kearney M, Palmer S, Maldarelli F, Shao W, Polis MA, Mican J, et al. Frequent polymorphism at drug resistance sites in HIV-1 protease and reverse transcriptase. AIDS 2008; 22:497-501; PMID:18301062; http://dx.doi.org/10.1097/QAD.0b013e3282f29478
48. Gerasimova YV, Kolpashchikov DM. Detection of bacterial 16S rRNA using a molecular beacon-based X sensor. Biosens Bioelectron 2013; 41:386-90; PMID:23021850; http://dx.doi.org/10.1016/j.bios.2012.08.058
49. Gao Y, Li Y, Zou X, Huang H, Su X. Highly sensitive and selective detection of biothiols using graphene oxide-based "molecular beacon"-like fluorescent probe. Anal Chim Acta 2012; 731:68-74; PMID:22652266; http://dx.doi.org/10.1016/j.aca.2012.04.020
50. Xiao Y, Plakos KJI, Lou XH, White RJ, Qian JR, Plaxco KW, et al. An Electrochemical Sensor for Single Nucleotide Polymorphism Detection in Serum Based on a Triple-Stem DNA Probe. Angew Chem Int Ed 2009; 48:4354-8; http://dx.doi.org/10.1002/anie.200900369
51. Dixon JM, Taniguchi M, Lindsey JS. PhotochemCAD 2: a refined program with accompanying spectral databases for photochemical calculations. Photochem Photobiol 2005; 81:212-3; PMID:15571431; http://dx.doi.org/10.1562/2004-11-06-TSN-361.1
52. MacroModel, version 9.1, Schrödinger, LLC, New York, NY 2005.
53. Weiner SJ, Kollman PA, Case DA, Singh UC, Ghio C, Alagona G. A new force field for molecular mechanical simulation of nucleic acids and proteins. J Am Chem Soc 1984; 106:765-84; http://dx.doi.org/10.1021/ja00315a051
54. Weiner SJ, Kollman PA, Nguen DT, Case DA. An All Atom Force Field for Simulations of Proteins and Nucleic Acids. J Comput Chem 1986; 7:230-52; http://dx.doi.org/10.1002/jcc.540070216